AFRL-AFOSR-VA-TR-2019-0163

Nonequilibrium Kinetics in High-Enthalpy Air

Thomas Schwartzentruber
REGENTS OF THE UNIVERSITY OF MINNESOTA

05/03/2019
Final Report

Air Force Research Laboratory
AF Office Of Scientific Research (AFOSR)/ RTB2
Arlington, Virginia 22203
Air Force Materiel Command

DISTRIBUTION A: Distribution approved for public release.

REPORT DOCUMENTATION PAGE

Form Approved
OMB No. 0704-0188

1. REPORT DATE *(DD-MM-YYYY)*	2. REPORT TYPE	3. DATES COVERED *(From - To)*
24-06-2019	Final Performance	01 Feb 2016 to 31 Jan 2019

4. TITLE AND SUBTITLE
Nonequilibrium Kinetics in High-Enthalpy Air

5a. CONTRACT NUMBER

5b. GRANT NUMBER
FA9550-16-1-0161

5c. PROGRAM ELEMENT NUMBER
61102F

6. AUTHOR(S)
Thomas Schwartzentruber

5d. PROJECT NUMBER

5e. TASK NUMBER

5f. WORK UNIT NUMBER

7. PERFORMING ORGANIZATION NAME(S) AND ADDRESS(ES)
REGENTS OF THE UNIVERSITY OF MINNESOTA
200 OAK ST SE 224
MINNEAPOLIS, MN 55455-2009 US

8. PERFORMING ORGANIZATION REPORT NUMBER

9. SPONSORING/MONITORING AGENCY NAME(S) AND ADDRESS(ES)
AF Office of Scientific Research
875 N. Randolph St. Room 3112
Arlington, VA 22203

10. SPONSOR/MONITOR'S ACRONYM(S)
AFRL/AFOSR RTB2

11. SPONSOR/MONITOR'S REPORT NUMBER(S)
AFRL-AFOSR-VA-TR-2019-0163

12. DISTRIBUTION/AVAILABILITY STATEMENT
A DISTRIBUTION UNLIMITED: PB Public Release

13. SUPPLEMENTARY NOTES

14. ABSTRACT
The proposed research focuses on developing predictive capability for nonequilibrium air dissociation in hypersonic flows. The most widely used dissociation rates were obtained from only a few experiments performed in the 1960s and 70s, where rates vary between 1-2 orders of magnitude. The present model (the Park TTv model) has been in widespread use for many years, despite known deficiencies. The overall goal of the proposed research is to completely replace such empirical models with new CFD models for air dissociation based on first-principles quantum chemistry calculations.
This involves four main objectives: (i) the use of quantum mechanical electronic structure calculations to develop new potential energy surfaces (PESs) for N2 and O2 collisions with N2, O2, NO, N, and O (ii) globally fitting the surfaces (iii) calculating collision dynamics as well as the internal energy state relaxation and dissociation processes resulting from the dynamics; and (iv) collecting the vast amount of new information generated from these first-principles calculations into new computational fluid dynamics (CFD) models for widespread use in the aerothermodynamics community.

15. SUBJECT TERMS
Aerothermodynamics, DSMC, quantum chemistry

16. SECURITY CLASSIFICATION OF:			17. LIMITATION OF ABSTRACT	18. NUMBER OF PAGES	19a. NAME OF RESPONSIBLE PERSON
a. REPORT	b. ABSTRACT	c. THIS PAGE			BERMAN, MICHAEL
Unclassified	Unclassified	Unclassified	UU		

Standard Form 298 (Rev. 8/98)
Prescribed by ANSI Std. Z39.18

				19b. TELEPHONE NUMBER *(Include area code)* 703-696-7781

Final Grant Report April 30th, 2019

FA9550-16-1-0161 - Nonequilibrium Kinetics in High-Enthalpy Air

Dr. Michael Berman: Molecular Dynamics and Theoretical Chemistry

Dr. Ivett Leyva: Aerothermodynamics

by

Thomas E. Schwartzentruber
Professor
Aerospace Engineering and Mechanics,
University of Minnesota

Phone: 612-625-6027 Fax: 612-626-1558 Email: schwart@umn.edu

Co-PIs: Prof. Don Truhlar and Prof. Graham Candler (University of Minnesota)

Period of performance: **February 1, 2016 – January 31th, 2019**

ABSTRACT AND OBJECTIVES FROM PROPOSAL:

The proposed research focuses on developing predictive capability for nonequilibrium air dissociation in hypersonic flows. The most widely used dissociation rates were obtained from only a few experiments performed in the 1960s and 70s, where rates vary between 1-2 orders of magnitude. The present model (the Park TT_v model) has been in widespread use for many years, despite known deficiencies. The overall goal of the proposed research is to completely replace such empirical models with new CFD models for air dissociation based on first-principles quantum chemistry calculations.

This involves **four main objectives**: **(i)** the use of quantum mechanical electronic structure calculations to develop new potential energy surfaces (PESs) for N_2 and O_2 collisions with N_2, O_2, NO, N, and O **(ii)** globally fitting the surfaces **(iii)** calculating collision dynamics as well as the internal energy state relaxation and dissociation processes resulting from the dynamics; and **(iv)** collecting the vast amount of new information generated from these first-principles calculations into new computational fluid dynamics (CFD) models for widespread use in the aerothermodynamics community.

Report Contents:

Journal publications (12):

Singh, N. and Schwartzentruber, T.E., "Non-Equilibrium Internal Energy Distributions During Dissociation", *PNAS – Proceedings of the National Academy of Sciences,* (2018), Vol. 115, No. 1, pp. 47-52.

Grover, M.S., Torres, E.M., and Schwartzentruber, T.E., "Direct Molecular Simulation of Internal Energy Relaxation and Dissociation in Oxygen", *submitted to Phys. of Fluids*, April, 2019.

Z. Varga, K. A. Parker, and D. G. Truhlar, "Direct diabatization based on nonadiabatic couplings: the N/D method" *Phys. Chem. Chem. Phys.*, 20, 26643 (2018).

M.S. Grover, T.E. Schwartzentruber, Z. Varga, and D.G. Truhlar, "Vibrational Energy Transfer and Collision-Induced Dissociation in O + O_2 Collisions" *J. Thermophys. Heat Tr.*, doi.org/10.2514/1.T5551

Y. Paukku, Z. Varga, and D.G. Truhlar, "Potential energy surface of triplet O_4" *J. Chem. Phys.*, 148, 124314 (2018).

Chaudhry, R.S., Bender, J.D., Schwartzentruber, T.E., and Candler, G.V., "Quasiclassical Trajectory Analysis of Nitrogen for High-Temperature Chemical Kinetics", *Journal of Thermophysics and Heat Transfer*, Vol. 32, No. 4, pp. 833-845 (2018).

Jaffe, R.L., Grover, M.S., Venturi, S., Schwenke, D.W., Valentini, P., Schwartzentruber, T.E., Panesi, M., "Comparison of Potential Energy Surface ad Computed Rate Coefficients for N_2 Dissociation", *Journal of Thermophysics and Heat Transfer*, Vol. 32, No. 4, pp. 869-881 (2018).

Macdonald, R.L., Grover, M.S., Schwartzentruber, T.E., and Panesi, M., "Construction of a coarse-grain quasi-classical trajectory method. II. Comparison against the direct molecular simulation method", *The Journal of Chemical Physics* 148, 054310 (2018)**.**

Schwartzentruber, T.E., Grover, M., and Valentini, P., "Direct Molecular Simulation of Nonequilibrium Dilute Gases", *Journal of Thermophysics and Heat Transfer*, Vol. 32, No. 4, pp. 892-903 (2018).

Y. Paukku, K.R. Yang, Z. Varga, G. Song, J.D. Bender, D.G. Truhlar, "Potential energy surfaces of quintet and singlet O4," *J. Chem. Phys.* 147, article no. 034301, pages 1-11 (2017).

Z. Varga, Y. Paukku, D.G. Truhlar, "Potential energy surfaces for O + O2 collisions," *J. Chem. Phys.* 147, article number 154312, pages 1–17 (2017).

Valentini, P., Schwartzentruber, T.E., Bender, J.D., and Candler, G.V., "Dynamics of nitrogen dissociation from direct molecular simulation", *Physical Review Fluids* (2016), Vol 1, 043402.

Conference Publications (16):

Jaffe, R.L, Schwenke, D.W., Grover, M., Valentini, P., Schwartzentruber, T.E., Venturi, S., and Panesi, M., "Comparison of quantum mechanical and empirical potential energy surfaces and computed rate coefficients for N2 dissociation", AIAA Paper 2016-0503, presented at AIAA SciTech 2016, San Diego, CA.

Valentini, P. and Schwartzentruber, T.E., "Ab initio based model for high temperature nitrogen rovibrational excitation and dissociation", AIAA Paper 2016-0500, presented at AIAA SciTech 2016, San Diego, CA.

Sing, N., Valentini, P., and Schwartzentruber, T.E., "A Coupled Vibration-Dissociation Model for Nitrogen from Direct Molecular Simulation", AIAA Paper 2016-4318, presented at AIAA Aviation 2016, Washington, DC.

Chaudhry, R., Bender, J.D, Valentini, P., Schwartzentruber, T.E., and Candler, G.V., "Analysis of Dissociation and Internal Energy Transfer in High Energy N2 + O2 Collisions Using the Quasiclassical Trajectory Method", AIAA Paper 2016-4319, presented at AIAA Aviation 2016, Washington, DC.

Grover, M., Schwartzentruber, T.E., and Jaffe, R.L., "Dissociation and internal excitation of molecular nitrogen due to N + N2 collisions using direct molecular simulation", AIAA Paper 2017-0660, presented at AIAA SciTech 2017, Grapevine, TX.

Macdonald, R.L., Grover, M., Schwartzentruber, T.E., and Panesi, M., "Coarse grain modeling and direct molecular simulation of nitrogen dissociation", AIAA Paper 2017-3165, presented at the 47th AIAA Thermophysics Conference, Aviation Forum, Denver, CO.

Chaudhry, R., Bender, J.D., Schwartzentruber, T.E., and Candler, G.V., "Quasiclassical Trajectory Analysis of N2+O2 and Implications for Hypersonic CFD", AIAA Paper 2017-3167, presented at the 47th AIAA Thermophysics Conference, Aviation Forum, Denver, CO.

Grover, M. and Schwartzentruber, T.E., "Internal energy relaxation and dissociation in molecular oxygen using direct molecular simulation", AIAA Paper 2017-3488, presented at the 47th AIAA Thermophysics Conference, Aviation Forum, Denver, CO.

Singh, N. and Schwartzentruber, T.E., "Coupled Vibration-Rotation Dissociation Model for Nitrogen from Direct Molecular Simulations", AIAA Paper 2017-3490, presented at the 47th AIAA Thermophysics Conference, Aviation Forum, Denver, CO.

Maninder S. Grover and Thomas E. Schwartzentruber. "Redistribution of Vibrational Energy: Mechanisms and Transition Probabilities", 2018 AIAA Aerospace Sciences Meeting, AIAA SciTech Forum, (AIAA 2018-1231).

Maninder S. Grover, Thomas E. Schwartzentruber, Zoltan Varga, and Donald G. Truhlar. "Dynamics of vibrational energy excitation and dissociation in oxygen from direct molecular simulation", 2018 AIAA Aerospace Sciences Meeting, AIAA SciTech Forum, (AIAA 2018-0238).

Robyn L. Macdonald, Maninder S. Grover, Thomas E. Schwartzentruber, and Marco Panesi. "State-to-State and Direct Molecular Simulation Study of energy transfer and dissociation in nitrogen mixtures", 2018 AIAA Aerospace Sciences Meeting, AIAA SciTech Forum, (AIAA 2018-0239).

Ross S. Chaudhry, Maninder S. Grover, Jason D. Bender, Thomas E. Schwartzentruber, and Graham V. Candler. "Quasiclassical Trajectory Analysis of Oxygen Dissociation via O2, O, and N2", 2018 AIAA Aerospace Sciences Meeting, AIAA SciTech Forum, (AIAA 2018-0237)

Ross S. Chaudhry and G.V. Candler, “Statistical Analyses of Quasiclassical Trajectory Data for Air Dissociation”, 2019 AIAA SciTech Forum, (AIAA 2019-0789).

Torres, E. and Schwartzentruber, T.E., “Direct molecular simulation of dissociating nitrogen in an adiabatic reactor”, AIAA Paper 2019-1049, presented at the AIAA Aerospace Sciences Meeting, SciTech Forum, San Diego, CA.

Grover, M.S. and Schwartzentruber, T.E., “Direct Molecular Simulation of Oxygen Dissociation”, 31st International Symposium on Rarefied Gas Dynamics, to appear in AIP Conf. Proc. (2019).

1.0 Potential Energy Surface (PES) Development (12 new PESs completed)

1.1 Summary:

In the past three years, we continued the development of ground-state potential energy surfaces (PESs) for collisions of the key atmospheric molecules (N_2 and O_2) and atoms (N and O). At this point, PESs have been completed for N_2+N_2, N+N_2, O_2+O_2, O+O_2, N_2+O_2, and N_2+O collisions corresponding to the ground electronic state. Surfaces are available online via POTLIB [http://comp.chem.umn.edu/potlib/].

Unlike N_2–N_2 and N_2–O_2 four-body systems, for which PESs were already published during a previous grant, the-ground state collision of two O_2 molecules can occur on surfaces with more than one possible spin quantum number. Since both O_2 collision partners are in triplet states in their ground states, they generate singlet, triplet, and quintet overall spin states when they collide. Similarly, the collision of ground-state O_2 molecule ($^3O_2$) with a ground-state O atom (^3O) can generate singlet, triplet, and quintet overall spin states. In the collision of ground state O_2 molecule ($^3O_2$) with a ground state N atom (^4N), the collision partners generate doublet, quartet, and sextet overall spin states.

From the point of view of mot previous chemistry-oriented studies, the low-energy spin states have been more interesting; therefore the chemistry-related literature is devoted mainly to the lowest spin states of these atmospheric species. But for a study of the high-energy collisions needed to understand the flow around hypersonic vehicles, the whole set of energetically accessible spin states is important, especially if we take into account that the higher-spin states have higher statistical weights than the lower-spin states. Using only a single surface or a subset of all the important surfaces might lead to incorrect energy-transfer distributions and incorrect dissociation rate constants. To address this issue, in our work we have provided complete sets of PESs for all the surfaces accessed in electronically adiabatic collisions of the ground state of $^3O_2$ molecule with another $^3O_2$ molecule and for all the surfaces accessed in electronically adiabatic collisions of the ground state of $^3O_2$ molecule with a ground-state ^3O atom. The description of collisions of $^3O_2$ molecule with a ground-state ^4N atom is still in progress.

1.2 Potential energy surfaces of O_4

We have developed potential energy surfaces (PESs) for collisions of O_2 molecules. The electronically adiabatic collision of $^3O_2$ with $^3O_2$ generates quintet, triplet, and singlet states, with respective statistical weights of 5, 3, and 1. We first worked on global ground-state potential energy surfaces for each these three spin states of O_4 for use in describing high-energy vibrational-rotational energy transfer and collision-induced dissociation in O_2-O_2 collisions. Due to the intrinsically multiconfigurational characters of oxygen and ozone molecules, construction of the potential energy surfaces is very challenging from the theoretical point of view, and it requires the application of multi-reference methods. Therefore, we used multi-state complete-active-space second-order perturbation theory (MS-CASPT2) with scaled external correlation (SEC) based on dynamically weighted SCF calculations and the maug-cc-pVTZ basis set to properly describe the interaction of O_2 molecules with other diatomic molecules or atoms as well as interactions of O_3 and an atom.

We have completed the potential energy surfaces for quintet, triplet, and singlet O_4 four-body systems. The singlet and triplet surfaces were published in one paper [Y. Paukku, K.R. Yang, Z. Varga, G. Song, J.D. Bender, and D.G. Truhlar, J. Chem. Phys., 147, 034301 (2017)] and the triplet surface was published in another paper [Y. Paukku, Z. Varga, and D.G. Truhlar, J. Chem. Phys. 148, 124314 (2018)]. The global six-dimensional O_4 PESs are fitted using least-squares fits to the many-body component of the electronic energies based on permutationally invariant polynomial basis functions in mixed exponential–Gaussians as bond-order variables. In the fitting procedure the diatomic potential energy curves are included as separate terms and these diatomic potential contain a damped dispersion correction for the O_4 PESs; the dispersion term makes the surface slightly more accurate at long-range interaction region, but for high-energy collisions its effect is less important than the treatment of the repulsive walls of the PESs. The surfaces we developed are being used for dynamical simulations to get reaction rate constants and energy transfer rate constants to model heat transport.

1.3 Potential energy surfaces of O_3

Collisions of O_2 molecules with O atoms are of great interest very important in high-enthalpy air. Although our ground-state singlet, triplet, and quintet O_4 surfaces contain O_3 as a subsystem, in those surfaces the spin state of the sub-fragments is not constrained (we only constrain the resultant spin state of the whole four-body system, which is conserved in the absence of spin-orbit coupling). Since the spin states of the subsystems are not maintained in the O_4 PESs as the geometry changes, the electron configuration (including spin state combinations) is selected that leads to the lowest possible energy, namely, the ground state, but this is not necessarily the PES that is accessed in O + O_2 collisions. Therefore further work was needed to prepare surfaces for studying O + O_2 collisions.

In the literature, only the singlet global PESs of the O_3 (ozone) system was previously reported. For studies of ozone production or decay in the atmosphere, this is the most important surface. But for the collision of $^3O_2$ with ^3O, the set of singlet surfaces have only a small statistical weight (1/9), since the collision generates quintet, triplet, and singlet spin states (three of each) with statistical weights for the three sets of spins being 5, 3, 1, respectively. Furthermore, the collision of O_2 with O involves three PESs for each spin symmetry, due to the threefold degenerate P character of the oxygen atom. Thus, altogether nine unique potential energy surfaces need to be developed to describe all possible electronically adiabatic collision events, and the weights on the surfaces are 5/27, 5/27, 5/27, ⅓, ⅓, ⅓, 1/27, 1/27, and 1/27, respectively. Considering these weights, it is easy to see that using only the ozone singlet surface, which has a weight of 1/27 in O + O_2 collisions, is inadequate.

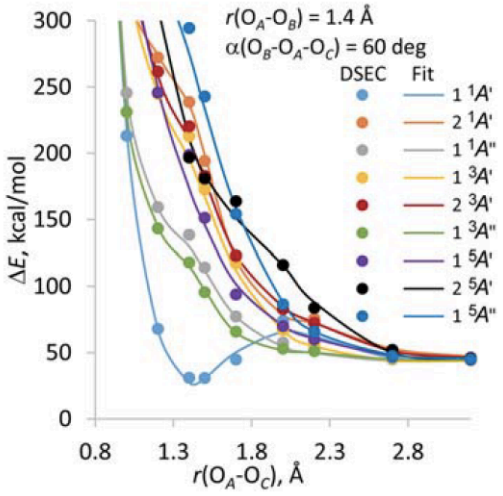

Fig. 1.1: Example cuts of the nine PESs for O3 collisions.

We have developed these nine global potential energy surfaces for adiabatic electronic states of O_3 [Z. Varga, Y. Paukku, D.G. Truhlar, J. Chem. Phys. 147, 154312 (2017)]. Namely 1 $^1A'$, 2 $^1A'$, 1 $^1A''$, 1 $^3A'$, 2 $^3A'$, 1 $^3A''$, 1 $^5A'$, 2 $^5A'$, and 1 $^5A''$, where, for instance, 2 $^3A'$ means the second adiabatic electronic state of triplet A' symmetry representation. Example results showing energy points and polynomial fits are shown in Fig. 1. These are the states of O_3 that are accessed in electronically adiabatic collisions of ground-state triplet O_2 molecule with ground-state triplet O atom. The surfaces are based on extended multi-state complete-active-space second-order perturbation theory (XMS-CASPT2) calculations with dynamically scaled external correlation (DSEC). The adiabatic surfaces are fitted to analytic functions using a many-body expansion where the pairwise additive term is fitted to an accurate diatomic potential including a damped dispersion term, and the many-body part, without disconnected terms, is fitted with permutationally invariant polynomials in mixed exponential-Gaussians to the electronic structure data points. The selection and weighting of points for the fits is designed to produce surfaces suitable for describing energy transfer and dissociation in high-energy collisions.

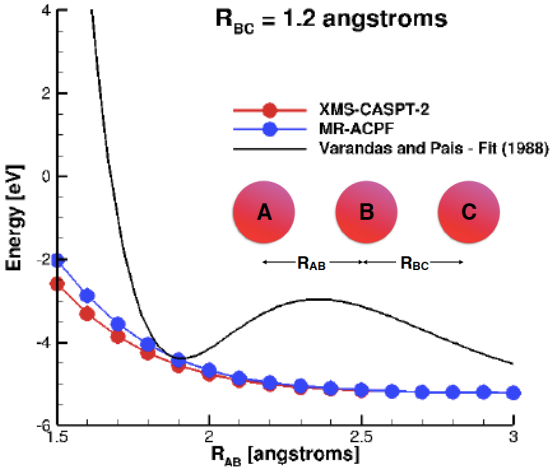

Fig. 1.2: Energy comparison between Varandas-Pais O_3 surface and new high-level electronic structure calculations, highlighting spurious energy maxima.

In a subsequent work [M. S. Grover, T. E. Schwartzentruber, Z. Varga, and D. G. Truhlar, J. Thermophys. Heat Tr., doi.org/10.2514/1.T5551], which mainly focuses on vibrational energy transfer and collision-induced dissociation in $O + O_2$ collisions, we compared a previous PES of the ozone surface by Varandas and Pais[i] with our newly developed surface and very significant differences were found. After investigating the development details of the Varandas-Pais surface, we found the source of the surface differences. The region of the Varandas-Pais surface corresponding to linear and nearly-linear geometries is based on extrapolated data, which were obtained from outdated electronic structure calculations. Besides the surface–surface comparison, high-level electronic structure calculations were carried out, which eventually confirm that the Varandas-Pais surface is problematic. This is shown in Fig. 1.2, where spurious (false) energy maxima are present in the Varandas-Pais surface. As detailed in section 3, these maxima inhibit exchange reactions and, as a result, predict a vibrational energy relaxation rate that is 10x too slow. The Varandas-Pais surface has been widely used in the hypersonics community.

1.4 Potential energy surfaces of NO_2

NO_2 potential energy surfaces have been a subject of many investigations due to their important role in atmospheric chemistry and combustion processes. The ground-state collision of O_2 molecule with N atom generates doublet, quartet and sextet spin state surfaces. Since the molecule is a sigma state ($^3\Sigma_g^-$) at its ground state, and the atom is a ^{4}S state its ground state, the electronically adiabatic collisions occur on a single surface if spin-orbit coupling is neglected (as it has been in all of our work to date, as justified by the low atomic numbers of the atoms involved). Note that, the ground-state collision of NO($^2\Pi$) with O(^{3}P) requires six states for doublet and quartet spin states. Only one of these six states connects to the ground state at the $O_2(^3\Sigma_g^-)$ + N(^{4}S) asymptote; the other five are excited states there. For six states, the diabatic representation of the PESs is more suitable than the adiabatic representation. However, we are not ready to carry out the adiabatic-to-diabatic transformation yet. Thus, altogether three (a doublet, a quartet, and a sextet) unique potential energy surfaces are being developed to describe the $O_2(^3\Sigma_g^-)$ + N(^{4}S) collisions in an adiabatic representation, namely the surfaces generated in electronically adiabatic collisions of $O_2(^3\Sigma_g^-)$ with N(^{4}S).

The construction of these single-state NO_2 surfaces involves electronic structure calculations based on the MS-CASPT2 method with maug-cc-pVTZ basis set and the application of dynamically scaled external correlation (DSEC). Most of the electronic structure calculations are done. The analytic functional form of the PES uses a many-body expansion with permutationally invariant polynomials in mixed exponential-Gaussians and without disconnected terms, and it has pairwise additive potentials as separate terms. The pairwise additive terms are fitted to an accurate diatomic potentials including a damped dispersion term. For doublet and quartet surfaces, the $O_2(^3\Sigma_g^-)$ and NO($^2\Pi$) diatomic potentials are used. But the combination of O(^{3}P) and NO($^2\Pi$), as an asymptotic limit, cannot correspond to a sextet spin state, thus the lowest energy quartet spin state of NO, namely the NO($^4\Pi$) diatomic potential is used instead of NO($^2\Pi$) for the sextet surface.

Preliminary surface fittings have been carried out for all three surfaces. Currently we are testing the quality of the fitted surfaces in several ways. This includes carrying out sample trajectory runs and comparing the geometries of PESs along the trajectories to electronic structure calculation and comparing the properties of stationary points of the PESs to known or specifically calculated values. We expect to finish the surfaces and publish them and make them available to our coworkers soon.

2.0 Nitrogen analysis

2.1 Summary:

Although the nitrogen PES and quasi-classical-trajectory (QCT) results were completed under a previous MURI grant, finalized results for nitrogen were obtained during the first year of this grant. In order to compute vibrational relaxation time constants and non-equilibrium dissociation rates (in Quasi-Steady-State – QSS), the Direct Molecular Simulation (DMS) technique is required. Details of such DMS calculations are described in section 5 (Fig. 5.2a for example). The DMS method accounts for non-Boltzmann internal energy distributions during quasi-steady-state (QSS) dissociation, which is the expected physics behind the strong shock waves present in the experiments. The findings below are published in the following papers:

Valentini, P., Schwartzentruber, T.E., Bender, J.D., and Candler, G.V., "Dynamics of nitrogen dissociation from direct molecular simulation", Physical Review Fluids, Vol. 1, 043402 (2016).

Chaudhry, R.S., Bender, J.D., Schwartzentruber, T.E., and Candler, G.V., "Quasiclassical Trajectory Analysis of Nitrogen for High-Temperature Chemical Kinetics", *Journal of Thermophysics and Heat Transfer*, Vol. 32, No. 4, pp. 833-845 (2018).

Jaffe, R.L., Grover, M.S., Venturi, S., Schwenke, D.W., Valentini, P., Schwartzentruber, T.E., Panesi, M., "Comparison of Potential Energy Surface ad Computed Rate Coefficients for N_2 Dissociation", *Journal of Thermophysics and Heat Transfer*, Vol. 32, No. 4, pp. 869-881 (2018).

Schwartzentruber, T.E., Grover, M., and Valentini, P., "Direct Molecular Simulation of Nonequilibrium Dilute Gases", *Journal of Thermophysics and Heat Transfer*, Vol. 32, No. 4, pp. 892-903 (2018).

2.2 Vibrational relaxation rates in nitrogen

Figure 2.1 shows the vibrational relaxatoin rates computed using DMS for both N_2+N_2 collisions and N+N_2 collisions. The important result is that the vibrational relxation due to N+N_2 collisions is approximately 10x faster than for N_2+N_2 collisions. This is due to the fact that atomic nitrogen promotes frequent exchange reactions $N^a + N^bN^c \rightarrow N^aN^b + N^c$. The post-collision N_2 molecule can have a substantially different vibrational energy state compared to the pre-collision molecule. In this manner, the presence of atomic nitrogen and associated exchange reactions lead to faster vibrational excitation. This 10x difference is not captured by current models (the Millikan-White correlations – blue lines – shown in Fig. 1). This difference is consistent with recent work from other groups using state-to-state analysis. The new models developed under the current grant for nitrogen (see section 6), use this more-accurate relaxation rate information.

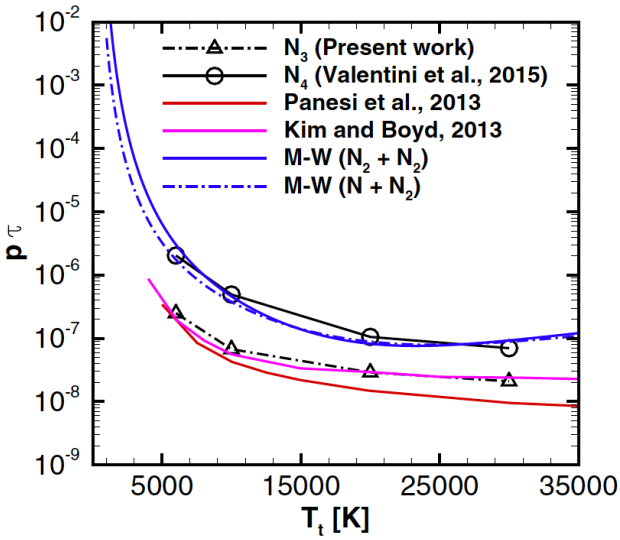

Fig. 2.1: Vibrational energy relaxation rates predicted by DMS (current work) and compared to existing correlations and recent results from other researchers.

2.3 Dissociation rates in nitrogen

Figure 2.2 shows comparisons of thermally averaged dissociation rate predictions compared to experimental shock-tube data. Computational results are presented for two different potential energy surfaces (PESs), used within the DMS simualtions; a PES from the Truhlar group at the University of Minnesota (UMN) and the PESs developed at NASA Ames.

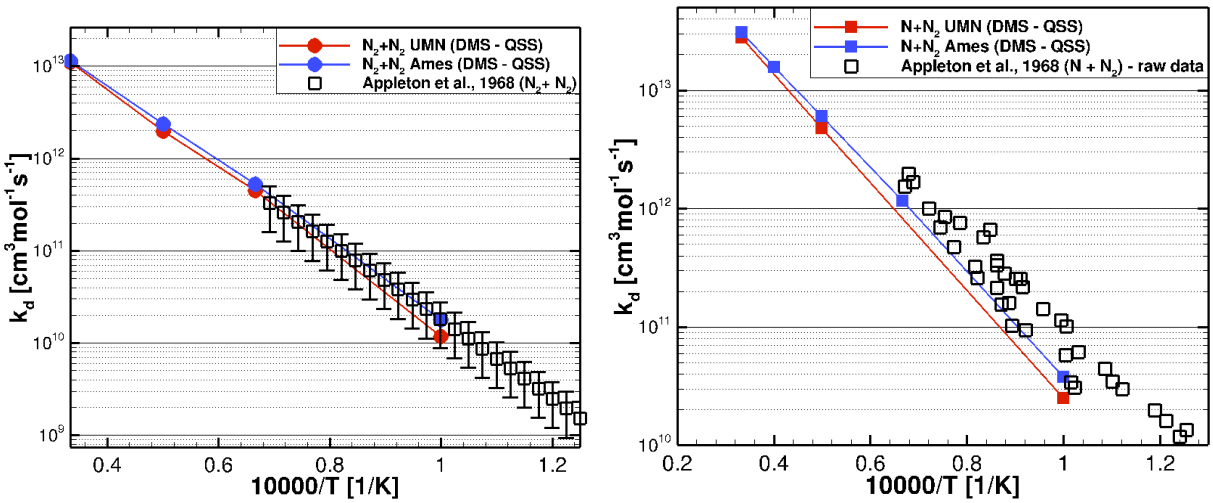

Figure 2.2 – (a) N_2+N_2 dissociation rates in QSS. (b) N+N_2 dissociation rates in QSS. Lines denote predictions using DMS using the PES from NASA and the PES from the Truhlar group at UMN. Symbols denote experimental data from Appleton et al.

Rates inferred from shock-tube experiments can vary by up to ~5x between experimental runs, for the same post-shock temperature (T) condition. In Fig. 2.2, we plot either the raw data or the data with error bars, straight from the original experimental papers. Also, it is important to understand that each experimental data point required various models to interpret a dissociation rate from spectroscopic measurements (other shock tube experiments interpret rates from end wall pressure-trace measurements). Considering the experimental uncertainties, our ab-initio predictions agree well with the data of Appleton. Other researchers in our field tend to claim that the Appleton data is the most accurate, since they used laser diagnostics instead of pressure-traces. However, to our knowledge this cannot be rigorously established. If data from other shock-tube experiments is included, the variation between experimental data points becomes more than an order of magnitude for the same post-shock temperature condition. Finally, Fig. 2.2 includes DMS results using both Truhlar PESs and NASA-Ames PESs for nitrogen. This gives an indication of the uncertainty in our ab-initio results. Here, two independent, high-quality PESs were developed and are found to produce very similar predictions.

It should be noted that there is much more to the story than the thermally averaged dissociation rates plotted in Fig. 2.2. The new models, described in sections 5 and 6, are predictive for general nonequilibrium conditions. Comparisons between the new models and traditional models (i.e. Park models) are also shown in section 6 for nitrogen.

3.0 Oxygen analysis

3.1 Summary:

As described in section 1, twelve new PESs have been developed for oxygen collisions as part of this grant. These PESs have been used to investigate vibrational energy relaxation and dissociation due to both O_2+O_2 and O+O_2 collisions in the ground electronic state. Other researchers in the hypersonics community have used the Varandas-Pais PES (1988) for their O+O_2 studies and publications. Using the corresponding PES from Truhlar, we find that the Varandas-Pais PES is inaccurate (see Fig. 1.2 and related discussion). Furthermore, the Varandas-Pais PES accounts for only $1/27^{th}$ of all O+O_2 collisions (i.e. only 1 spin-configuration). In reality, there are 9 possible spin-configurations for O+O_2 and 3 spin-configurations for O_2+O_2. Using all 12 PESs for oxygen collisions, we find order-of-magnitude differences between different PESs (spin configurations). Therefore, all 12 PESs are indeed necessary to understand oxygen excitation and dissociation. This section presents final DMS results for oxygen, that agree well with available shock-tube data and provide the basis for new models described in sections 5 and 6. Details of such DMS calculations are described in section 5 (for example Fig. 5.2a). The DMS method accounts for non-Boltzmann internal energy distributions during quasi-steady-state (QSS) dissociation, which is the expected physics behind the strong shock waves present in the experiments. The findings below are published in the following papers:

Grover, M.S., Torres, E.M., and Schwartzentruber, T.E., "Direct Molecular Simulation of Internal Energy Relaxation and Dissociation in Oxygen", *submitted to Phys. of Fluids*, April, 2019.

Grover, M.S., Schwartzentruber, T.E., Varga, Z., and Truhlar, D.G., "Vibrational energy transfer and collision induced dissociation in O + O2 collisions", accepted for publication, to appear in the *Journal of Thermophysics and Heat Transfer* (2019).

3.2 Vibrational relaxation in rates in oxygen

For the single spin-state modeled by the Varandas-Pais PES, we find >10x difference in the vibrational relaxation time constant compared to that predicted by the corresponding Truhlar group PES (Fig. 3.1a). As detailed previously in section 1.3, the discrepancy is caused by the fact that the Varandas-Pais PES has spurious maxima in potential energy that are not real.

In Fig. 3.1b, we present our ab-initio DMS predictions, using *all* spin-state configurations, compared to experimental shock tube data for vibrational relaxation time constants. Overall, close agreement (both in magnitude and trend with temperature) is found between our predictions and experimental data for both O_2+O_2 and O+O_2. Similar to nitrogen, one main result is that the vibrational relxation due to O+O_2 collisions is approximately 10x faster than for O_2+O_2 collisions. This is due to the fact that atomic species promote frequent exchange reactions $O^a + O^bO^c \rightarrow O^aO^b + O^c$. The commonly used Park expression for O_2+O_2 relaxation is accurate, except at high temperatures where the relaxation becomes too fast compared to our calculations and experimental data. The Park expression for O+O_2 relaxation was fit to the Kiefer and Lutz data (and limited at high temperatures to give a physically reasonable rate). The trend with increasing temperature is noticeably different compared to the almost-constant trend found in our simulations The recent data from Ibraguimova et al. does not show raw-data or error bars in the journal paper. Again, our ab-initio simulations show that the reason the vibrational relaxation rate remains relatively constant with increasing temperature is because exchange collisions have a high probability (low energy barrier), leading to fast relaxation (small time constant) across a wide range of temperatures.

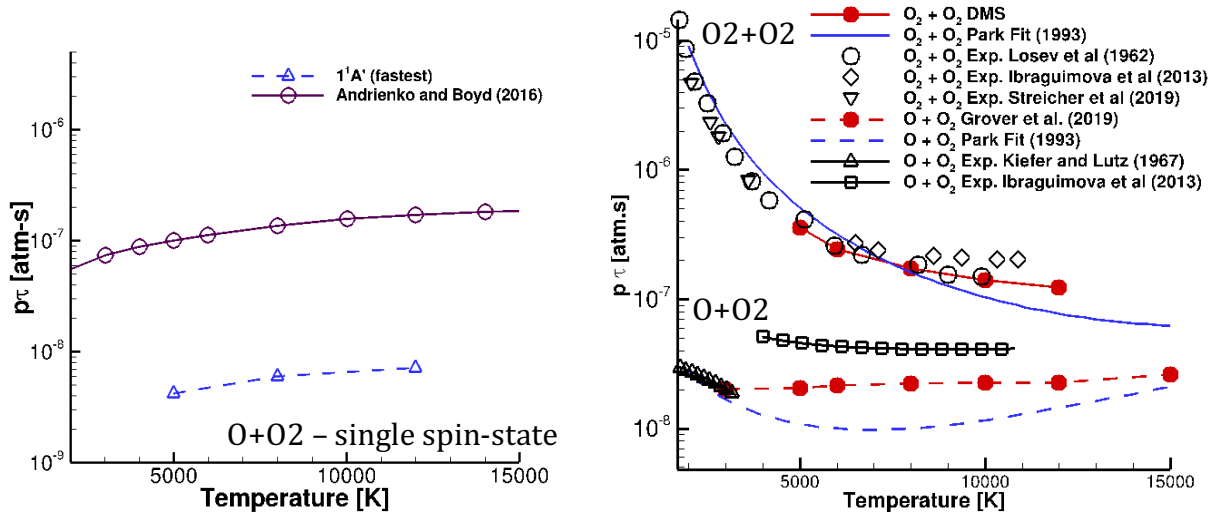

Figure 3.1 – (a) Vibrational relaxation time constant for $O+O_2$ collisions. Results are for only a single spin-state configuration (1 PES) and are compared between our results (using the Truhlar PES) and results from Andrienko and Boyd (using the Varandas-Pais PES). (b) Vibrational relaxation time constant for O_2+O_2 collisions (top portion) and $O+O_2$ collisions (bottom portion). Computational results use the DMS method with all spin-states simulated (3 PESs for O_2+O_2 and 9 PESs for $O+O_2$). Note that the Park expression (for $O+O_2$) was "fit" to the Kiefer/Lutz data.

3.3 Dissociation rates in oxygen

Table 3.1: Electronic states of molecular oxygen and corresponding degeneracies

State	Energy (eV)	Degeneracy
$X^3\Sigma_g^-$	-5.21	3
$a^1\Delta_g$	-3.84	2
$b^1\Sigma_g^+$	-3.15	1
$c^1\Sigma_u^-$	-1.02	1
$C^3\Delta_u$	-0.81	6
$A^3\Sigma_u^+$	-0.72	3
$B^3\Sigma_u^-$	1.14	3
$2^3\Pi_g$	1.98	6

Since the PESs used in this work correspond to the ground electronic state, the DMS predictions do not include effects of electronically excited states. However, it is likely that electronically excited states do influence the dissociation process in oxygen. As shown in Table 3.1, there are six electronic states that lie below the dissociation barrier (5.21 eV) [Saxon, R. P., and Liu, B., "Ab-initio configuration interaction study of the valence states of O2," The Journal of Chemical Physics, Vol. 67, No. 12, 1977, pp. 5432–5441]. A method to account for dissociation from electronically excited states has been proposed by Nikitin [Nikitin, E. E., "Theory of elementary atomic and molecular processes in gases," Oxford, Clarendon Press, 1974], where it is assumed that the time-scale for electronic and vibrational excitation are comparable at high temperatures. In this approach, all electronically excited states are assumed to be in equilibrium, and it is assumed that there will be equilibrium among vibrational levels of the electronically excited states. With these assumptions, dissociation would occur concurrently from the ground electronic state and the electronically excited states. An estimate of the overall dissociation rate is then obtained by multiplying the rate from the ground-state calculations by the sum of degeneracies of all the electronic states below the dissociation energy (including ground state) divided by the degeneracy of the ground state. This multiplication factor comes out to be $\eta = 16/3$ for classically bound molecules, and has been commonly used in recent work on oxygen dissociation. A more accurate method would be to perform electronically non-adiabatic trajectories and to include electronically excited O_2 states explicitly in the DMS simulation. However, this approach requires PESs describing the excited states as well as couplings between states, which are not presently available (discussed in section 7). Therefore, when dissociation

rate coefficients are presented, we present the predicted rates from DMS without the factor (i.e. ground electronic state results) and also with the $\eta = 16/3$ factor (i.e. the limiting case where dissociation occurs from all excited states below the dissociation energy).

Figure 3.2 presents the dissociation rate coefficients obtained by DMS calculations during QSS dissociation. The results are plotted for the limiting cases where the multi-surface factor is set to $\eta = 1$ (assuming no dissociation from electronically excited states) or it is set to $\eta = 16/3$ (assuming dissociation occurs from all electronically excited states below the dissociation energy). Figure 3.2a compares the dissociation rate coefficients obtained by DMS calculations with experimental data from Ibraguimova et al [Ibraguimova, et al., "Investigation of oxygen dissociation and vibrational relaxation at temperatures 4000-10,800 K," The Journal of Chemical Physics 139, 034317 (2013)], and new data from Streicher et al [Streicher, et al., "Measurements of oxygen vibrational relaxation and dissociation using ultraviolet laser absorption in shock tube experiments," in AIAA Scitech 2019 Forum (#2019-0795)]. Clearly, DMS predictions agree closely with the experimental data when the full multi-surface factor ($\eta = 16/3$) is assumed. This suggests that in the experiments, the low-lying excited states of O_2 are fully populated. On-going research involves generating PESs for the relevant electronically excited states of oxygen and performing non-adiabatic dynamics calculations to predict the rate of electronic excitation and populations of excited states behind strong shock waves (refer to section 7). However, direct experimental evidence of excited state populations is not currently available. Therefore, the results plotted in Fig. 3.2a only provide indirect evidence that the excited states of oxygen are populated, corresponding to use of the full multi-surface factor ($\eta = 16/3$). When these results are compared with rate coefficients obtained by Ibraguimova et al. (Fig. 3.2a), the DMS data agrees well at high temperatures with noticeable discrepancy below 6000 K. However, the DMS data is in close agreement, across the full range of temperatures studied, with the recent 2019 experimental data from Stanford of Streicher et al.

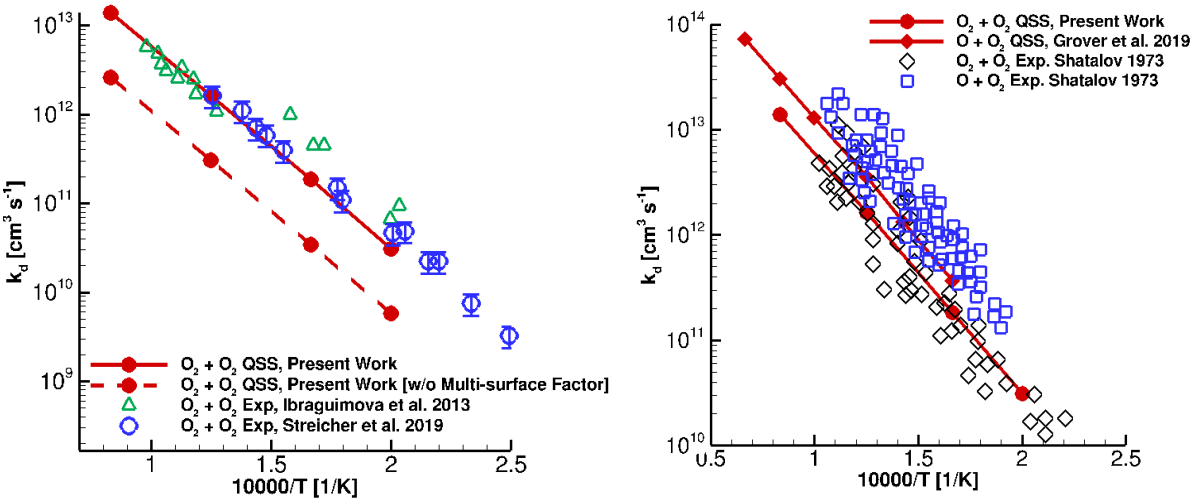

Figure 3.2 – (a) Comparison of dissociation rate coefficients for O_2+O_2 computed by DMS calculation using the PESs from the Truhlar group (limiting cases of no electronic excitation and full electronic excitation) with experimental data. (b) Comparison of rate coefficients computed by DMS (assuming full electronic excitation) with experimental data for both O_2+O_2 and O+O_2 by Shatalov.

In Fig. 3.2b, the DMS results are compared to the dissociation rate coefficients inferred from shock tube measurements made by Shatalov [Shatalov, "Molecular dissociation of oxygen in the absence of vibrational equilibrium," Combustion, Explosion and Shock Waves 9, 610-613 (1973)], where rates for both O_2 + O_2 and O + O_2 where inferred. While the experimentally inferred rates have substantial

uncertainty, there is a noticeable trend that dissociation proceeds faster when atomic oxygen is present compared to when the gas is comprised of mainly molecular oxygen. DMS results corresponding $O + O_2$ collisions, are plotted in Fig. 3.2b along with the DMS results corresponding to $O_2 + O_2$ collisions. The DMS calculations also predict faster dissociation in QSS when $O + O_2$ collisions are included (by a factor of approximately 2) in qualitative agreement with the experimental data. It is important to note that the uncertainty in the experimental data is quite large (Fig. 3b) and new experiments with lower uncertainty could provide a stronger validation of this finding.

4.0 N_2 + O_2 analysis

4.1 Summary:

The N2O2 PES described in section 1 was used to perform a large number of qausi-classical-trajectory (QCT) collision calculations between N_2 and O_2 species.

Chaudhry, R.S., Bender, J.D., Schwartzentruber, T.E., and Candler, G.V., "Quasiclassical Trajectory Analysis of Nitrogen for High-Temperature Chemical Kinetics", *Journal of Thermophysics and Heat Transfer*, Vol. 32, No. 4, pp. 833-845 (2018).

Overall, many of the physical mechanisms, such vibrational excitation rates, vibration-dissociation coupling, QSS states, etc.) are found to be similar compared to N_2+N_2 and O_2+O_2 collisions. However, there were two notable findings regarding N_2+O_2 collisions. First, the direct dissociation of N_2 and O_2 to form NO was found to have a relatively high reaction rate. This reaction is not even included in commonly used air dissociation rate sets (i.e. the Park model). Second, the commonly used Park reaction rate coefficient for O_2 dissociation due to N_2 appears to be too high when compared to existing experimental data and our calculations. Finally, the Zeldovich reactions, which are the primary mechanism of NO formation and play an important role in nitrogen dissociation, have been very well studied using computational chemistry in the literature (the BSUV flight experiments and modeling campaign), and were not studied in detail during the current grant.

4.2 Direct production of NO from N_2+O_2 collisions

A large number of QCT calculations have been performed for the N2O2 system, using the published PES developed by the Truhlar group. As shown in Fig. 4.1, an interesting result is that the dissociation-exchange reaction (N_2+O_2 → NO + N + O) was found to occur with significant frequency. In fact, this reaction was more probable at all temperatures than N_2 dissociation (N_2 + O_2 → 2N + O_2). This dissociation-exchange reaction (N_2+O_2 → NO + N + O) is not even included in current CFD models (i.e. the Park model). Figure 5 plots the equilibrium reaction rates, for various reactions, calculated by QCT. This reaction may be important during the early stages of dissociation where significant N_2 and O_2 is present. However, once an appreciable amount of O_2 dissociation occurs, the reaction N_2 + O → NO + N is expected to dominate. Sensitivity studies using CFD is the best method to determine which reactions are important and under what conditions.

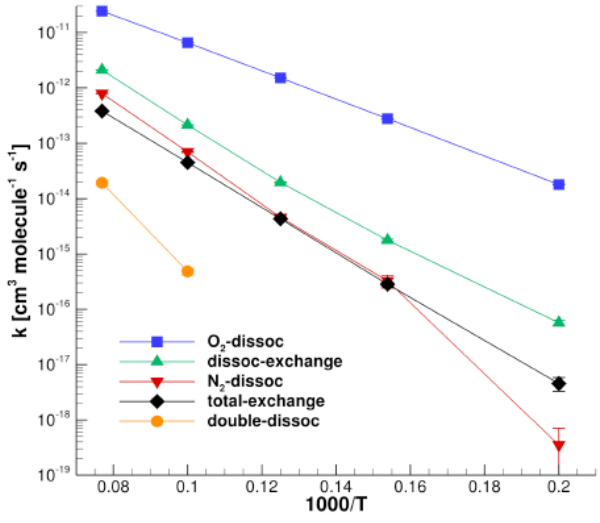

$$N_2 + O_2 \longrightarrow N_2 + O_2$$
$$N_2 + O_2 \longrightarrow N_2 + 2\,O \quad \text{(O-dissoc)}$$
$$N_2 + O_2 \longrightarrow 2\,N + O_2 \quad \text{(N-dissoc)}$$
$$N_2 + O_2 \longrightarrow NO + N + O \quad \text{(dissoc-exchange)}$$
$$N_2 + O_2 \longrightarrow 2\,NO \quad \text{(total-exchange)}$$
$$N_2 + O_2 \longrightarrow 2\,N + 2\,O \quad \text{(double-dissoc)}$$

Figure 4.1 – Equilibrium rate constants for various reactions involved in the N2O2 system as calculated by QCT. [Reproduced from Chaudhry, Bender, Schwartzentruber, and Candler, AIAA Paper 2017-3167]

4.3 Rate of O_2 dissociation due to N_2

Figure 4.2 compares available data in the literature to our results for the reaction $O_2 + N_2 \rightarrow O + O + N_2$. To our knowledge, there are only two experimental measurements of this reaction (from Generalov and Losev, and from Jerig et al.). Figure 4.2 also shows reaction rate fits by Bortner, in addition to the widely used Park rates. Finally, QCT results from our research and from Andrienko and Boyd (both studies used the N2O2 PES developed in the Truhlar group) are also shown in the plots. Specifically, Fig. 4.2a plots the rate constants versus inverse temperature, and Fig. 4.2b scales the y-axis by a baseline exponential in order to show more clearly the differences between experiments and various modeling results. As seen in Fig. 4.2b, Park's rate is too large compared to the experimental result of Generalov and Losev. Furthermore, the experimental data of Jerig et al., which was performed after Park's reinterpretation and had a primary goal of measuring this rate, found a rate that was much lower than the one described by Park. Therefore, based on the data from Jerig, and the predictions of QCT calculations at higher temperatures, that Park's recommendation for oxygen dissociation with partner N_2 is too high. At 4000 K, our prediction (labelled Present Work) is within a factor of 2 of both experimental measurements, which are themselves approximately a factor of 3 apart. At this condition, the Park rate is a factor of 5 higher than the present work. The differences are dependent on temperature, but our result is at least two times lower than the Park rate for the entire temperature range that the Park rates were initially quoted to be accurate (up to 7000 K). Our results are also similar to those of Andrienko and Boyd, who used the same N2O2 PES. Finally, it is important to note that these QCT studies assumed equilibrium (Boltzmann) internal energy distributions, corresponding to T, to initialize and sample collision statistics. We expect that the QSS state of O2 molecules would include depletion of high vibrational energy levels (refer to Fig. 5.2 for more details). This non-Boltzmann effect would further lower the predicted rates by a factor of approximately two, leading to an even greater difference compared to the commonly used Park rate.

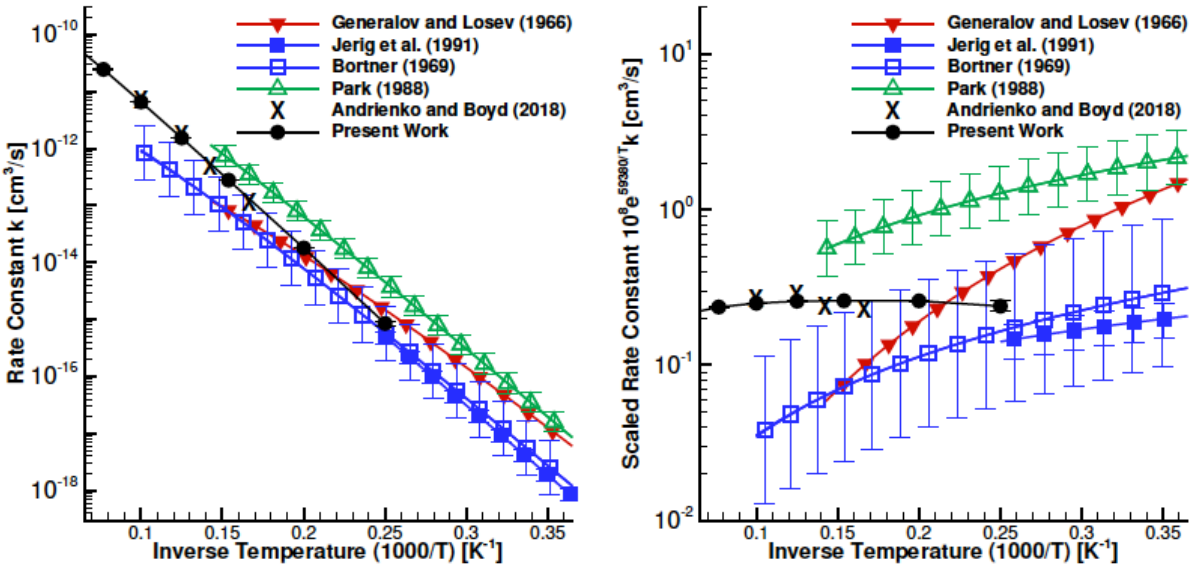

Figure 4.2 – Equilibrium rate constants for the reaction $O_2 + N_2 \rightarrow O + O + N_2$ determined by QCT calculations using the N2O2 PES developed by the Truhlar group. Results are compared to available experimental data and prior model expressions. [Reproduced from Chaudhry and Candler, AIAA Paper 2019-0789.]

5.0 Molecular Level Modeling and Non-Boltzmann Effects

5.1 Summary:

In this section, the details of the new dissociation model are summarized. Based on extensive QCT and DMS ab-initio calculation results we find the most important physical processes to model include (i) the influence of translational energy, rotational energy, and vibrational energy on dissociation, (ii) the distributions of rotational and vibrational energy in the gas, in addition to (iii) non-Boltzmann effects including overpopulation (and depletion) of high vibrational energy states during rapid excitation (and quasi-steady-state dissociation). Importantly, we find that these physical processes can be modeled accurately with relatively simple expressions and that pre-computing millions of state-to-state energy transitions is clearly unnecessary. We develop simple models for these processes that are both accurate and yield an analytical closed-form continuum rate expression for use in CFD.

5.1 Dissociation rate formulation (what are the important modeling aspects?)

The multi-temperature dissociation rate expression is written as follows [Truhlar and Muckerman (1979) Atom-Molecule Collision Theory, (Springer, New York), pp 505–566]:

$$K(T,\langle\epsilon_{rot}\rangle,\langle\epsilon_v\rangle) = \frac{1}{S}\left(\frac{8k_BT}{\pi\mu_C}\right)^{1/2}\sum_{v=0}^{v_{\max}}\sum_{j=0}^{j_{\max}}\int_0^\infty p(d|\epsilon_{rel},\epsilon_{rot},\epsilon_v)\pi b_{\max}^2\left(\frac{\epsilon_{rel}}{k_BT}\right)\exp\left[-\frac{\epsilon_{rel}}{k_BT}\right]d\left(\frac{\epsilon_{rel}}{k_BT}\right)f(\epsilon_{rot})f(\epsilon_v)$$

(1) probability given trans, rot, vib, energies

translational energy distribution (known equilibrium)

(2) distribution of rot, vib, energies (non-Boltzmann)

Whereas the widely used Park model uses $K(T_{eff})$, where $T_{eff} = (T\ Tv)^{1/2}$, we have developed a more general expression that is a function of translational temperature T, average rotational energy $<\varepsilon_{rot}>$, and average vibrational energy $<\varepsilon_v>$. While the Park model is an empirical fit based on limited experimental data and is inconsistent with computational chemistry, the model we have formulated is purely predictive (not fit to experiment at all) and analytically derived using kinetic theory.

As denoted in the above expression, there are two main aspects that we need to model. **(1)** We need an accurate model for the probability of dissociation given the translational, rotational, and vibrational energy involved in the collision, and **(2)** We need an accurate model for the distributions of rotational and vibrational energy states in the gas (non-Boltzmann). Both of these models are discussed in the next two sections.

5.2 Probability of dissociation given rotational and vibrational energies

Based on billions of collisions computed using QCT and DMS methods, we find very clear trends for the probability of dissociation. Specifically, we find that the probability of dissociation has an exponential dependence on rotational energy and vibrational energy. As a result, we propose the following simple, yet accurate, model for the probability:

$$p(d \mid \epsilon_{rel},\epsilon_v,\epsilon_{rot}) = C_1\left[\frac{\epsilon_{rel}+\epsilon_{int}-\epsilon_d^{\text{eff}}}{\epsilon_d}\right]^\alpha\frac{\epsilon_d}{\epsilon_{rel}}\exp\left[\beta\frac{\epsilon_{rot}}{\epsilon_d}\right]\exp\left[\gamma\frac{\epsilon_v}{\epsilon_d}\right],\quad \epsilon_{rel}+\epsilon_{int}\geq\epsilon_d^{\text{eff}}$$

The first term captures the dependence on the relative translational energy (ε_{rel}), and ensures there is enough collision energy compared to the required dissociation energy (also accounting for the effective centrifugal barrier). This term is modeled as a power-law with a fitting parameter α. The second term captures the exponential dependence on rotational energy with fitting parameter β. The third term captures the exponential dependence on vibrational energy with fitting parameter γ.

Figures 5.1a, b, and c, show just how accurate this simple expression is. The model is able to accurately capture a huge amount of QCT collision data (refer to each figure caption for details). The exponential dependence of the dissociation probability on rotational and vibrational energy is clearly evident in Figs. 5.1b and 5.1c. **A general conclusion to draw from Fig. 5.1 is that pre-computing millions of state-to-state probabilities (cross-sections) does not appear necessary at all. Rather, simple expressions can very accurately capture the QCT data and trends.**

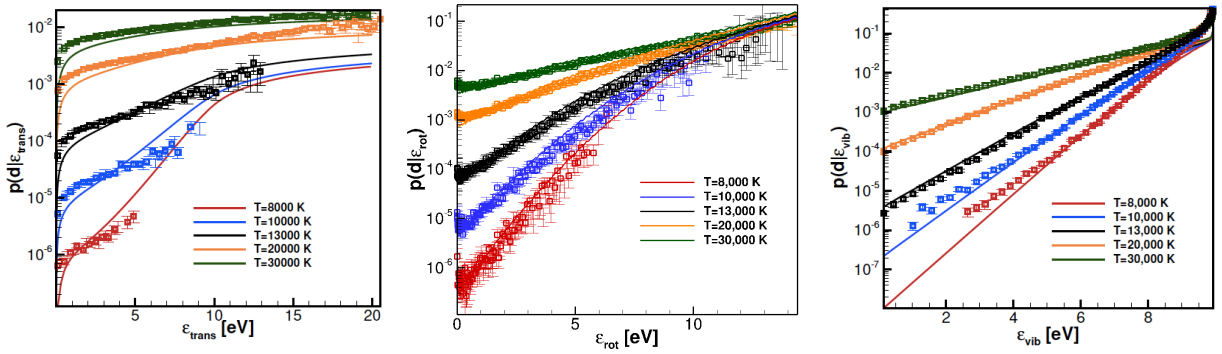

Figure 5.1 – (a) Probability of dissociation versus relative translational energy (averaged over equilibrium distributions for rotational and vibrational energy corresponding to various *T*). (b) Probability of dissociation versus rotational energy (averaged over equilibrium distributions for translational and vibrational energy corresponding to various *T*). (c) Probability of dissociation versus vibrational energy (averaged over equilibrium distributions for translational and rotational energy corresponding to various *T*). Symbols represent QCT collision results. Lines represent model expression results.

5.3 Distribution functions for rotational and vibrational energies (non-Boltzmann)

Now that we have a model for the probability of dissociation, given the translational, rotational, and vibrational energies involved in the collision, we need to integrate this probability expression over the distributions of rotational and vibrational energy states in the gas [$f(\varepsilon_{rot})$, $f(\varepsilon_v)$]. DMS and master-equation calculations clearly show that the internal energy distribution functions are non-equilibrium (non-Boltzmann). For example, Fig. 5.2a shows the a DMS simulation where nitrogen gas rapidly excites to 20,000 K. The gas rotational and vibrationally excites and then reaches a Quasi-Steady-State (QSS) dissociation regime. Figure 5.2b shows the vibrational energy distribution functions at various times during this process, where the symbols are the DMS raw data and the lines represent the corresponding equilibrium (Boltzmann) distribution at each time.

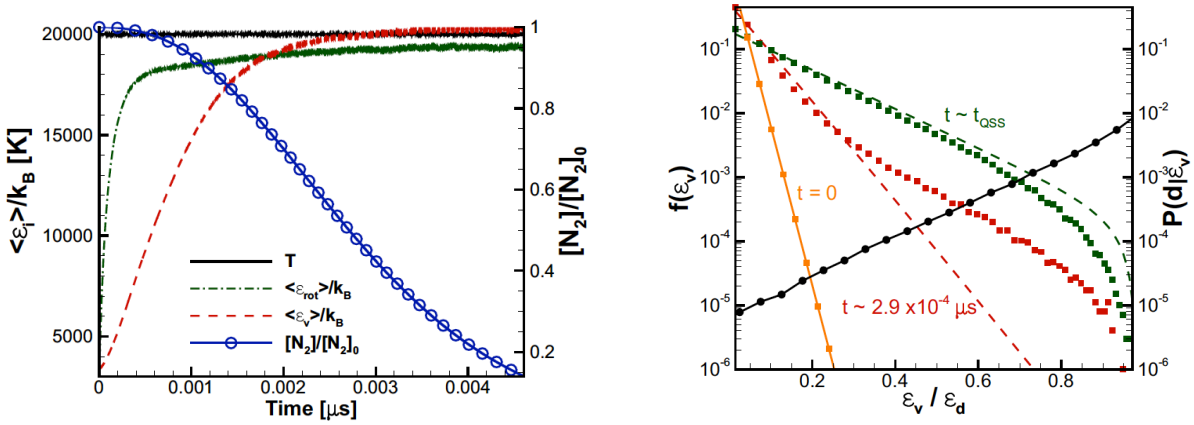

Figure 5.2 – (a) Example DMS results for rovibrational excitation and dissociation at 20,000K. Average energy and concentration histories are plotted. (b) Vibrational energy distribution functions at various times corresponding to the calculation in shown in Fig. 5.2(a). Symbols are DMS data, lines represent the corresponding equilibrium distributions (Boltzmann).

There are two aspects of non-Boltzmann energy distributions that require modeling. The first is the **overpopulation** of high-energy states (compared to Boltzmann) during the early rapid excitation phase (the red line and symbols in Fig. 5.2b). In this phase, if a Boltzmann distribution was assumed, the dissociation rate would be under-predicted since the high-energy states are exponentially more likely to dissociate. The second aspect is the **depletion** of high-energy states (compared to Boltzmann) during the QSS dissociation phase (the green line and symbols in Fig. 5.2b). In this phase, if a Boltzmann distribution was assumed, the dissociation rate would be over-predicted, again, since the high-energy states are exponentially more likely to dissociate. For reference, the black line (right axis) shows the probability of dissociation versus vibrational energy, which spans four orders of magnitude. Therefore, if we are to accurately capture non-Boltzmann effects, we must capture the degree of overpopulation during rapid excitation and the degree of depletion during QSS.

This problem was solved by Singh and Schwartzentruber in the paper [Singh and Schwartzentruber, "Non-Equilibrium Internal Energy Distributions During Dissociation", *Proceedings of the National Academy of Sciences,* Vol. 115, No. 1, pp. 47-52 (2018).]. Specifically, we are able to capture both the overpopulation and depletion discussed above (and seen in Fig. 5.2b), with a simple model based on surprisal analysis:

$$-\log\left[\frac{f(\epsilon_v)}{f_0(\epsilon_v)}\right] = \lambda_0 + \lambda_1 \frac{\langle\epsilon_t\rangle}{\epsilon_d} v + \lambda_2 \left(\frac{\langle\epsilon_t\rangle}{\langle\epsilon_v\rangle} - \frac{\langle\epsilon_v\rangle}{\langle\epsilon_t\rangle}\right)^{\psi} v$$

Here, $f(\varepsilon_v)$ is the nonequilibrium vibrational energy distribution function and $f_0(\varepsilon_v)$ is the Boltzmann distribution based on the average of ε_v. In surprisal analysis (a well established theory in the literature), the deviation from Boltzmann is modeled as a measure of entropy deficiency, which is minimized subject to constraints on the system. We assume the two main constraints include (i) depletion due to dissociation (proportional to the average translational energy $\langle\varepsilon_t\rangle$ compared to the dissociation energy ε_d) and (ii) overpopulation due to excitation (proportional to the difference between average translational and vibrational energy, $\langle\varepsilon_t\rangle - \langle\varepsilon_v\rangle$). With only two free parameters (λ_1 and λ_2), we find that all of the non-Boltzmann distributions found by DMS can be accurately predicted with this simple model. This is shown in Fig. 5.3(a)-(c).

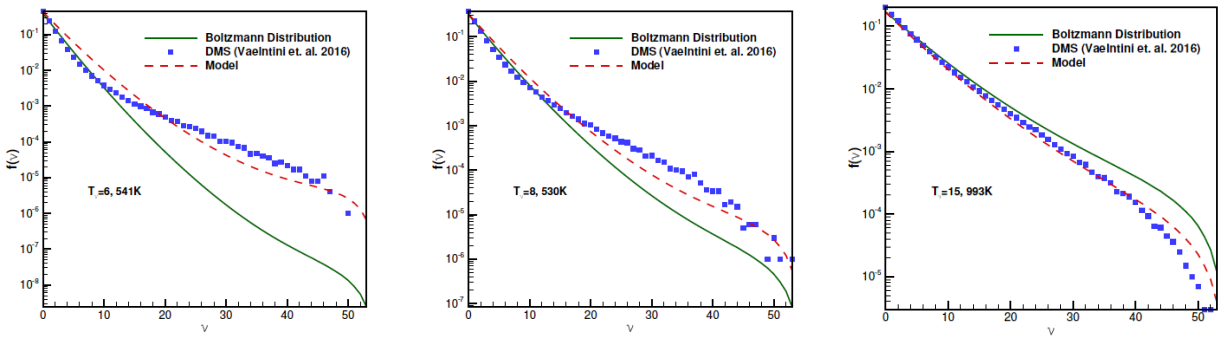

Figure 5.3 – (a),(b) Non-Boltzmann vibrational energy distribution functions during rapid excitation, exhibiting overpopulation of the high-energy tail. (c) Non-Boltzmann vibrational energy distribution function, exhibiting depletion of the high-energy tail. DMS data, model results, and Boltzmann distributions are compared.

To summarize, based on QCT and DMS data using PESs from the Truhlar group, we have developed accurate (yet simple) model expressions for both the probability of dissociation in function of the rotational and vibrational energies involved in a collision, and the distribution functions of rotational and vibrational energy (including non-Boltzmann effects). In fact, the simple model expressions can be integrated to yield a new closed-form, analytical, expression for the dissociation rate that can be used in large-scale CFD simulations. This is described in the next section.

6.0 New Continuum-Level Dissociation Model

6.1 Summary:

In this section, a new continuum-level dissociation rate expression is described, which is analytically obtained by integrating the molecular models (described in section 5). Therefore, no new free parameters are introduced and the molecular and continuum models are mathematically consistent. The new continuum model captures (i) the influence of translational energy, rotational energy, and vibrational energy on dissociation, (ii) the distributions of rotational and vibrational energy in the gas, in addition to (iii) non-Boltzmann effects including overpopulation (and depletion) of high vibrational energy states during rapid excitation (and quasi-steady-state dissociation). New model results are compared with the standard Park models, and new model results are also compared with QCT and DMS ab-initio results. It is noted that much of the mathematical analysis is omitted for brevity, and that some of the model equation parameters and notation may change after final publication.

6.2 Functional form of new dissociation model

The Park model is a standard Arrhenius rate model but uses an `effective' temperature (T_{eff}) that is empirically set as the geometric mean of T and T_v:

$$k(T,T_V) = AT_{eff}^{\eta}\ \exp\left[-\frac{\varepsilon_d}{k_B T_{eff}}\right], \quad T_{eff} = \sqrt{T\ T_V}$$

In contrast, our new model derives analytically from kinetic theory, combined with the molecular-level model expressions based on QCT/DMS ab-initio results. Specifically, combining the equations in sections 5.1, 5.2, and 5.3, one can analytically derive the following dissociation rate expression:

$$k(T,T_{rot},T_v) = AT^{\eta}\exp\left[-\frac{\epsilon_d}{k_B T}\right] * [\mathrm{H}(\epsilon_d,0,1) + \mathrm{H}(\epsilon_d^{\max},\epsilon_d,2)]$$

$$\eta = \alpha - \frac{1}{2}; \qquad A = \frac{1}{S}\left(\frac{8k_B}{\pi\mu_C}\right)^{1/2}\pi b_{\max}^2 C_1 \Gamma[1+\alpha]\left(\frac{k_B}{\epsilon_d}\right)^{\alpha-1}$$

$$\mathrm{H}(x,y,n) = \frac{\exp[(-1)^{n-1}}{\mathrm{Z}^{QSS}(T_{rot},T_v)}\frac{\exp\left[x\delta_{rot}\right]\mathrm{g}^{QSS}(\delta_{vr}) - \exp\left[y\delta_{rot}\right]\mathrm{g}^{QSS}(\delta_v - y\delta_{rot}/\epsilon_d)}{k_B\theta_{rot}\delta_{rot}};$$

where

$$\delta_{rot} = -\frac{1}{k_B T_{rot}} + \frac{1}{k_B T} + \frac{\beta - \theta_{CB} + (-1)^n\delta}{\epsilon_d} - \frac{\theta_{CB}}{k_B T} + \frac{\delta_{rot}^{NB}}{\theta_{rot}k_B};$$

$$\delta_v = -\frac{1}{k_B T_v} + \frac{1}{k_B T} + \frac{\gamma + (-1)^n\delta}{\epsilon_d} + \frac{\delta_v^{NB}}{\theta_v^m k_B} \qquad \delta_{vr} = \delta_v - \delta_{rot}$$

While the details of the derivation and full description of all terms is omitted for brevity, a few aspects of the model warrant discussion. First, the new model consists of a standard Arrhenius rate expression based on the translation temperature, T. The influence of rotational and vibrational energy on the dissociation rate is contained in a separate term, $H = H(T, T_{rot}, T_v)$. The function H contains effects due to the average rotational and vibrational energy state of the gas, as well as non-Boltzmann effects. The two H terms contain the contribution from bound molecules and quasi-bound molecules, respectively. Second, the parameter α is seen to appear in the translational temperature exponent, the parameter β appears in the rotational energy contribution term, and the parameter γ appears in the vibrational energy contribution

term. Recall, from section 5.2 that these parameters were based on QCT data and therefore no additional free parameters have been introduced in the above continuum rate expression. In fact, as expected from the exponential dependence described in section 5.2, the controlling function H consists of exponential functions containing contributions from rotational energy δ_{rot} and vibrational energy δ_v. Third, non-Boltzmann effects due to overpopulation and depletion simply appear as additional individual terms δ_v^{NB} and δ_{rot}^{NB}, which are simple functions of λ_1 and λ_2 from section 5.3. Fourth, it is noted that the final notation used for the new model expressions is currently being finalized for publication. Although the notation of some terms and parameters may change before final publication, the above expressions represent the finalized functional form with all required model dependencies.

While the above dissociation rate expression may appear to be complex, it is important to note that it is simply a function of T, T_{rot}, and T_v (as well as a number of molecular parameters based on QCT and DMS results). Therefore, this expression can be used in standard large-scale CFD simulations (especially if trans-rotational equilibrium is assumed: $T = T_{rot}$). In fact, section 6.4 outlines how, under reasonable assumptions, this model can be further simplified. Finally, since the new model is analytically derived from kinetic theory, DSMC and CFD models should now agree precisely in the near-continuum limit (a necessity for a hybrid CFD-DSMC code).

6.3 New Model Results

The above dissociation model is now compared to QCT and DMS calculation results. Figure 6.1 shows the model results, assuming Boltzmann internal energy distributions by neglecting δ_v^{NB} and δ_{rot}^{NB} terms, compared to the QCT results of Bender et al. Since these results correspond to Boltzmann distributions, Fig. 6.1 is showing the dramatic effect that *average* vibrational energy (parameterized by T_v) has on the dissociation rate. While the Park model uses $T_{eff} = (T\,T_v)^{1/2}$ to capture this, the new model accurately captures this effect through the function $H(T,T_{rot},T_v)$. The paper by Bender et al. [Bender, et al. "An improved potential energy surface and multi-temperature quasiclassical trajectory calculations of $N_2 + N_2$ dissociation reactions", *J. Chem. Phys.* (2015), 143, 054304] contains comparison to the Park model where significant differences are found compared to QCT data under certain conditions.

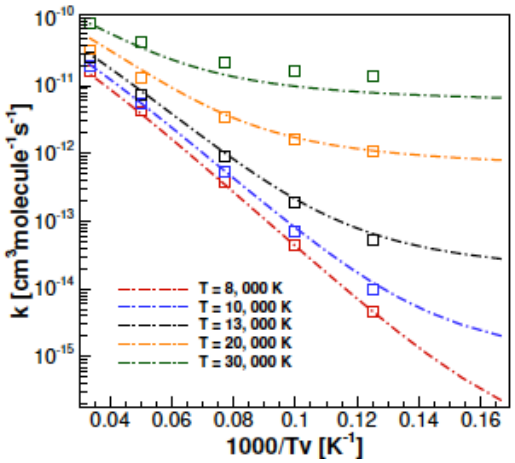

Fig. 6.1: Nitrogen dissociation rates under thermal nonequilibrium conditions (but assuming Boltzmann distributions). QCT data compared to model results.

The energy removal due to dissociation reactions is also a critical quantity required by a CFD model. This quantity can be analytically determined from the dissociation rate expression, and therefore, no additional free parameters are introduced. While the details are omitted for brevity, essentially, this quantity captures the fact that molecules with high vibrational energy are exponentially more likely to dissociate. Figure 6.2a shows QCT results for the vibrational energy removal due to nitrogen dissociation compared to three existing models from the literature. None of the existing models accurately captures the correct trend. In contrast, as shown in Fig. 6.2b, the new model accurately reproduces the QCT data.

Perhaps the most important comparisons are shown in Fig. 6.3. A zero-dimensional relaxation integration code was developed to test the new continuum models. This allows us to directly compare both standard Park model results (which use the non-preferential energy removal model in Fig. 6.2) and new model results with DMS calculations for rovibrational excitation and dissociation. Figure 6.3a shows significant differences between the Park model solution and the results of DMS for nitrogen dissociation. Note that

the plots show average rotational energy and vibrational energy (not T_{rot} and T_v), and that although temperatures are expected to approach an equilibrium value, the average energies in rotational and vibrational modes are not expected to asymptote to the same value. The most important discrepancy is that the effective dissociation rate predicted by the Park model is significantly faster than the DMS result. One main reason for this difference is that the non-preferential energy removal does not remove enough vibrational energy from the gas, resulting in a much higher average vibrational energy, and therefore a higher rate of dissociation. This difference in average vibrational energy between the Park model solution and DMS is also evident in Fig. 6.3a (note that the Park model assumes trans-rotational equilibrium). In contrast, Fig. 6.3b shows that the new model agrees closely with the DMS result for rotational energy content, vibrational energy content, and the rate of dissociation.

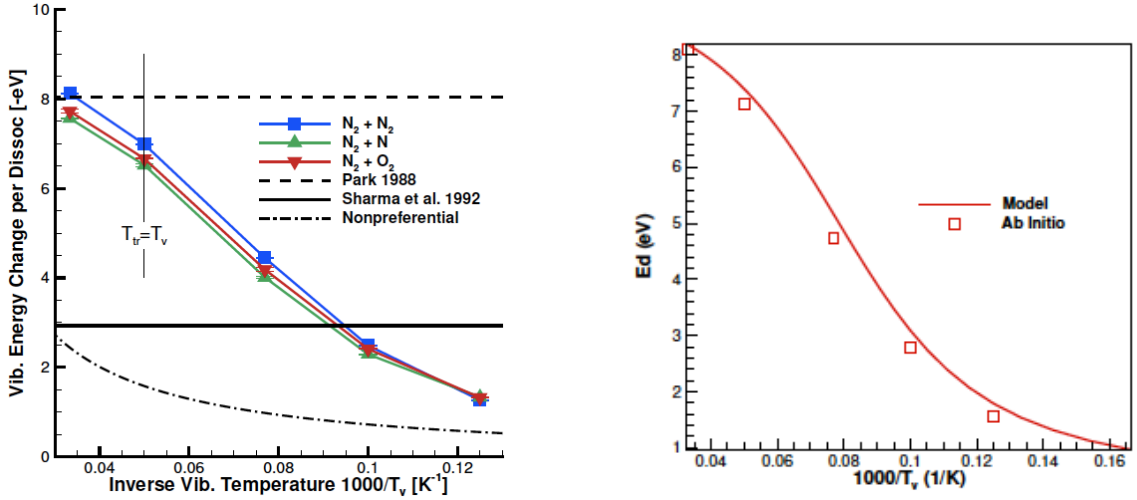

Figure 6.2 – (a) Vibrational energy loss due to dissociation vs. inverse vibrational temperature. QCT data is plotted as symbols for various collision partners, and compared to existing models from the literature. (b) The QCT data for N_2-N_2 from Fig. 6.2a is compared to results using the new dissociation model.

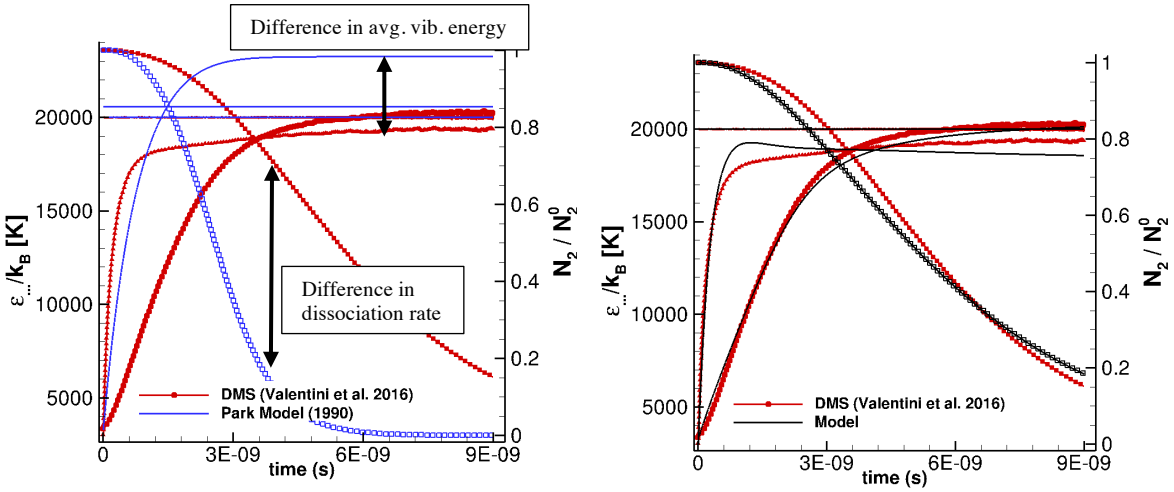

Figure 6.3 – Zero-dimensional rovibrational excitation and dissociation in nitrogen. (a) Park model results compared to DMS ab-intio results. (b) New model results compared to DMS ab-initio results.

Finally, the new models have been implemented into the US3D CFD code without any significant increase in computational cost. As an example demonstrating its use, Fig. 6.4 shows US3D simulations of Mach 19.6 nitrogen flow (inviscid) over a 7 degree half-angle sphere-cone at 40 km altitude. Simulations

are performed using current state-of-the-art CFD models for vibrational energy relaxation and dissociation (labeled "Standard Park") and are also performed using the new models described above. As seen by the translational temperature contours (Figs. 6.4a and 6.4b), the new model predicts a similar flow structure as the Park model, as expected. However, as seen in Figs. 6.4c and 6.4d, the details of thermochemical state (notably the vibrational temperature contours) are dramatically different. The vibrational temperature predicted by the standard models is approximately 2000 K higher than that predicted by the new model for most of the flow field. This is due primarily to the fact that the new model correctly removes more vibrational energy (since it is the highly excited molecules that dissociate) and also promotes faster translational-vibrational energy transfer (thereby equalizing the temperatures) due to the proper modeling of exchange reactions. These discrepancies are consistent with the zero-dimensional excitation comparison in Fig. 6.3a. This example demonstrates that we have reached the point of running full CFD simulations with our new models and that there are significant differences compared to the Park model.

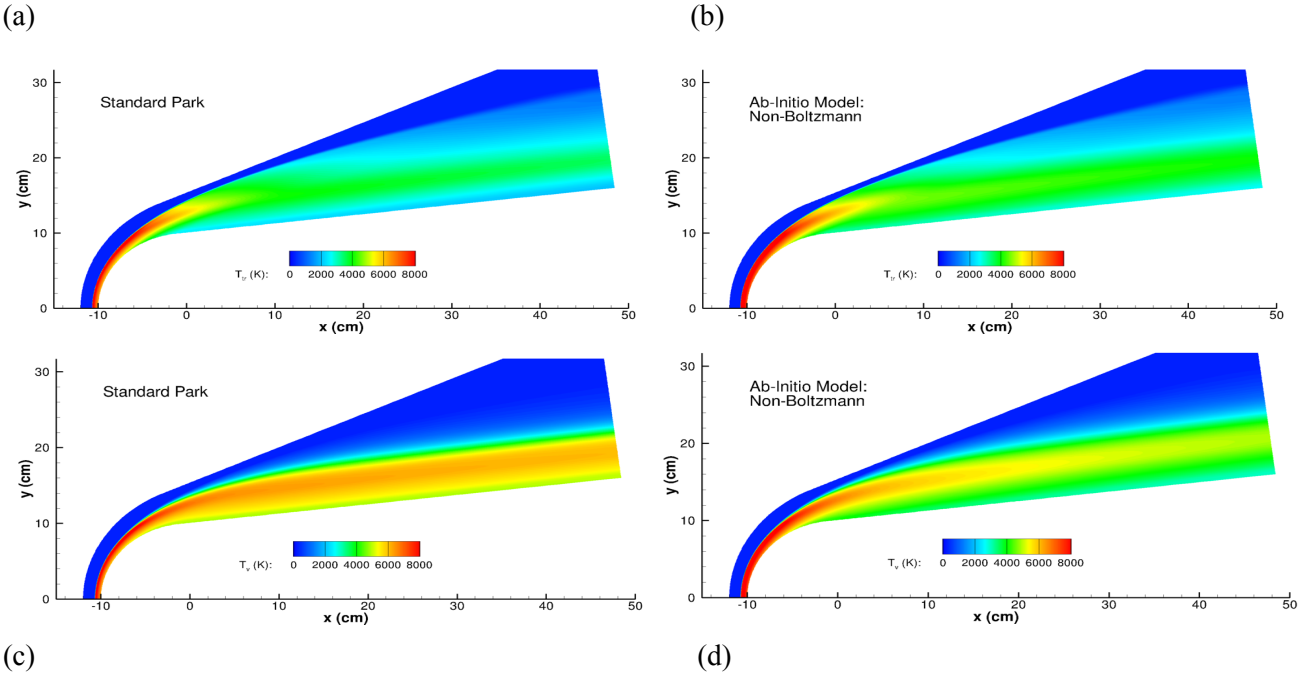

Figure 6.4 – US3D simulation of hypersonic nitrogen flow over a sphere-cone. Translational temperature contours for Park (a) vs. new model (b). Vibrational temperature contours for Park (c) vs. new model (d).

6.4 Reduced Model

The new dissociation model described in section 6.2 captures what we consider to be the relevant physical processes. Upon further investigation, we have been able to quantify the importance of the various processes on macroscopic results of most interest (the overall dissociation rate, for example). We find that a number of simplifying assumptions can be made, resulting in an even more efficient model for large-scale CFD simulation. As an example, Fig. 6.5 shows the new model results compared to DMS, but now assuming trans-rotational equilibrium and also ignoring non-Boltzmann overpopulation effects. Despite making these assumptions, the model agreement with DMS remains very good. In fact, comparing the agreement of the full model (Fig. 6.3b) with the agreement in Fig. 6.5, one could argue that the discrepancy is certainly acceptable and the difference may not even be measureable by current experimental techniques.

Figure 6.3 – Zero-dimensional rovibrational excitation and dissociation in nitrogen. *Reduced* model results compared to DMS ab-initio results.

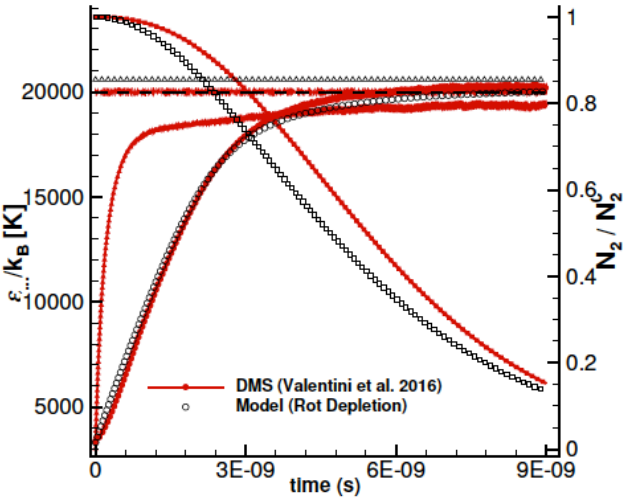

Mathematically, it can be shown that under the assumptions of trans-rotational equilibrium, neglecting the effect of overpopulation on dissociation, but maintaining the QSS depletion effect, the full model expression resembles the model by Morrone and Treanor [Marrone and Treanor, "Chemical relaxation with preferential dissociation from excited vibrational levels", The Physics of Fluids, 6(9):1215-1221, 1963]. As recently presented and analyzed by Chaudhry and Candler [Chaudhry and Candler, AIAA Paper #2019-0789], the Marrone and Treanor (M-T) model has the following form.

$$Z\left(T_{\mathrm{tr}}, T_{\mathrm{v}}\right) = \frac{k_{\mathrm{d}}\left(T_{\mathrm{tr}}, T_{\mathrm{v}}\right)}{k_{\mathrm{d}}\left(T_{\mathrm{tr}}, T_{\mathrm{tr}}\right)}$$

Here, the function Z represents the nonequilibrium correction that is applied to standard Arrhenius reaction rate based on an equilibrium temperature, equal to the translational temperature T_{tr}. The function Z is a ratio of partition functions (often approximated) based on the various energy modes in the gas, along with an empirical parameter U:

$$\ln Z\left(T_{\mathrm{tr}}, T_{\mathrm{v}}\right) = \ln \mathrm{Q_v}\left(T_{\mathrm{tr}}\right) + \ln \mathrm{Q_v}\left(T_{\mathrm{F}}\right) - \ln \mathrm{Q_v}\left(T_{\mathrm{v}}\right) - \ln \mathrm{Q_v}\left(-U\right)$$

$$\frac{1}{T_{\mathrm{F}}} = \frac{1}{T_{\mathrm{v}}} - \frac{1}{T_{\mathrm{tr}}} - \frac{1}{U}$$

The recent conference paper by Chaudhry and Candler [Chaudhry and Candler, AIAA Paper #2019-0789], presents in detail how the free parameters in the M-T can be fit to provide close agreement with our QCT data over a wide range of conditions. Two aspects that are missing from the M-T model include the rotational contribution to the energy removal due to dissociation and the non-Boltzmann depletion effects relevant to the QSS state.

Using reasonably accurate assumptions, one can mathematically reduce the full model equation (presented in section 6.2) to the M-T functional form, where rotational effects and non-Boltzmann depletion effects are now present:

$$\frac{1}{k_B T_{F'}} = -\frac{1}{k_B T_v} + \frac{1}{k_B T_{rot}} + \frac{B_1}{\epsilon_d} + \frac{\theta_{CB}}{k_B T} - \frac{\delta_{rot}^{NB}}{k_B \theta_{rot}} + \frac{\delta_v^{NB}}{k_B \theta_v^{\mathrm{eff}}}$$

$$= -\frac{1}{k_B T_v} + \frac{1}{k_B T_{rot}} + \frac{1}{k_B U'} - \frac{\delta_{rot}^{NB}}{k_B \theta_{rot}} + \frac{\delta_v^{NB}}{k_B \theta_v^{\mathrm{eff}}} \qquad B_1 = \gamma - \beta + \theta_{CB}$$

Therefore, we have developed a new nonequilibrium model that contains all of the relevant physical processes (presented in section 6.2), and have shown that under certain reasonable assumptions a reduced model (similar to the M-T model) is obtained. CFD users may then have the option of implementing either (or both) models in their codes, depending on the level of accuracy and complexity desired.

7.0 Efforts towards NO2 and excited electronic states of oxygen

7.1 Diabatic Summary:

In addition to providing the PESs accessed in electronically adiabatic collisions of ground-state reagents, we have also started making preparation for working on PESs necessarily involved in collisions of electronically excited collision partners and in electronically nonadiabatic collisions of ground-state collision partners. Furthermore, we are calculating the couplings between the surfaces that are needed to model electronically nonadiabatic collisions. To treat the dynamics occurring on coupled PESs, it is convenient to express the surfaces and their couplings in electronically diabatic representations. The available electronic structure programs only provide adiabatic representations of the wave functions. In electronically adiabatic representations the electron configurations are not maintained along geometry changes, the state crossings in a given symmetry manifold are avoided along most paths, the energies of the states are only ordered entirely in terms of increasing energy, the PESs have multidimensional cuspidal ridges where the first derivatives are discontinuous, and the nonadiabatic couplings (NACs) are singular vectors along these ridges (which are called conical intersections). In a diabatic representation, the electron configurations are maintained, the energies of the different states cross each other smoothly, end the couplings are nonsingular scalars. For these reasons, the diabatic representation is more convenient for nonadiabatic dynamics. However, the adiabatic-to-diabatic transformation is not trivial, nor is it unique; and there is no generally successful diabatization prescription.

This problem of diabatization is still among the greatest challenges in theoretical chemistry. In our work on this project, we have developed a new diabatization scheme that has the potential to become a generally applicable method, and we consider this as an important accomplishment. This method uses the NACs and of the gradients of the adiabatic PESs without needed information at the conical intersections. The NACs are directly related to the expected crossings of the diabatic PESs. Although the usage of NACs is not easy, and we have found that both expected and unexpected difficulties, we are encouraged that progress may be possible. The method development is still ongoing. Besides this method, we have also investigated possible improvements of previously developed diabatization methods, including the DQΦ method. Finally, we have started to investigate the relation to diabatic states of the model states of extended multi-state complete-complete-active 2nd-order perturbation theory.

7.2 Diabatization of adiabatic surfaces

Our current and future work involves the calculation of excited states and their diabatization. Once we have the adiabatic wave functions of the ground electronic state and the low-lying electronically excited states provided by multireference electronic structure calculations, we can generate their diabatic representation and fit the couplings between the different surfaces. This allows conveniently running the nonadiabatic dynamics to study the energy transfer and the reactive collisions for the four-body systems and three-body subsystems. However, the adiabatic-to-diabatic transformation is not trivial and, based on our current tests, the available diabatization methods are not entirely suitable for our systems. Because of the highly open-shell character of nitrogen and oxygen atoms, several excited states are required in the calculation to describe even the first few electronic energy levels (due to near degeneracy in the interaction region). Although property-based diabatization is very powerful and successful for many problems, based on our tests, the properties of the electronic structures used in the currently available property-based diabatization techniques do not distinguish many of the states needed for our unusually difficult problem.

N/D diabatization method

We are developing a new diabatization method based on nonadiabatic coupling (NAC) matrix elements. The NACs (as geometry-dependent variables) carry information about how the wave functions of two electronic states are mixed along geometry changes; thus they are directly related to state crossings and locally avoided crossings along paths. Each NAC matrix element is a 3*N*-dimensional vector in the

Cartesian space, where N is the number of atoms in the system. It is known that for a simple two-state case that the gradient of adiabatic-to-diabatic rotation angle at a given geometry is the NAC vector of the state pair. In theory, if one can fit the NACs with suitable functions of geometry, then the integral of the function leads to the adiabatic-to-diabatic rotation angle, but in practice, this procedure is very cumbersome for various reasons. One of these reasons is the requirement is that the whole potential energy surface has to be fitted at once. This is not suitable of direct dynamics studies, and thus direct diabatization methods are preferred, where the diabatization of a given geometry point is (in a practical sense) independent of its environment. Our newly developed diabatization scheme belongs to the class of direct diabatization methods; and besides the NACs, the adiabatic energy gradients are used in the scheme. The core idea of the N/D diabatization method has been already published [Z. Varga, K. A. Parker, and D. G. Truhlar, Phys. Chem. Chem. Phys., 20, 26643 (2018)]. The name of the N/D method reflects the key step of matrix diagonalization by using Jacobi transformations, where the tangent of the rotation angle is calculated as a ratio of nonadiabatic elements (numerator) to derivatives of diagonal elements (denominator). An important advantage of the N/D diabatization method over property-based diabatization methods is that the NACs carry information about each state crossing, while a single property or combination of properties does not necessarily do that. Nevertheless, the N/D method still requires further work to overcome technical and theoretical difficulties. For example, the NACs carry information about rotation-introduced state couplings (Coriolis-couplings). This has not been widely studied or discussed in the literature, but we are examined a projection technique to deal with the problem. From the point of view of global potential energy surface fitting in the diabatic representation, these Coriolis-couplings are problematic and they have to be removed. We have already started addressing this issue by using projection operators.

Besides the Coriolis-couplings, the NACs can have other unphysical contributions. This is less problematic at crossing regions, where the contribution of the state crossing dominates. But for the most useful diabatic representations, there are regions where the diabats are equal to the adiabats and those unphysical contributions prevent that. They introduce spurious coupling effects. Thus, they have to be removed. We are investigating possible damping functions to deal with this issue.

Another problem of the published N/D diabatization scheme is the large number of user-selected variables, which makes finding useful diabatic states very complicated. This can be considered both as an advantage and as a disadvantage – the advantage is that (recalling that the diabatic states are not unique) the complications allow us to find the most useful diabatic representation for dynamics, provided we can keep the diabats smooth. Here, we also have made some progress, but further work is needed to decrease the number of user-dependent variables and make the application of the method simpler or at least more automatic.

After addressing the difficulties, the N/D method has a potential to become a generally successful diabatization technique for both surface fitting and direct dynamics purposes.

Extension of DQΦ method

Transition properties based on one-electron operators, for example the dipole (D), quadrupole (Q), or electrostatic potential (Φ), do not fully distinguish all the different states of our systems containing oxygen and nitrogen atoms. To make property-based diabatization approaches more flexible, a new property was added to the previous ones. The new transition properties are calculated based on the two-electron orbital angular momentum operator. Since it is a two-electron operator, it has the chance to overcome the limitation of one-electron operators and distinguish a larger number of states. The previously published *DQΦpac* program [C. E. Hoyer, L. Gagliardi, and D. G. Truhlar, "*DQΦpac, Version 2.0*", available for free at http://comp.chem.umn.edu/dqphipac] was extended read the data of the new transition properties, and the program was improved in other way too. The program was also renamed to *DiaProp* and it will be available on the website of Truhlar group soon [C. E. Hoyer, K. A. Parker, Z. Varga, L. Gagliardi, and D. G. Truhlar, "DiaProp: A program for diabatization based on

properties, Version 1.0", to be available for free at http://comp.chem.umn.edu/diaprop].

Other diabatization schemes

Besides the above-mentioned N/D method and *DiaProp* program, other diabatization ways have also been considered, but they have not been successful enough to discuss in detail at this time.